AD-A121 472 CONSTRAINTS ON TRANSPORTABLE ION BEAM POWER(U) NAVAL 1/1
RESEARCH LAB WASHINGTON DC P F OTTINGER ET AL.
12 NOV 82 NRL-MR-4948

UNCLASSIFIED F/G 20/7 NL

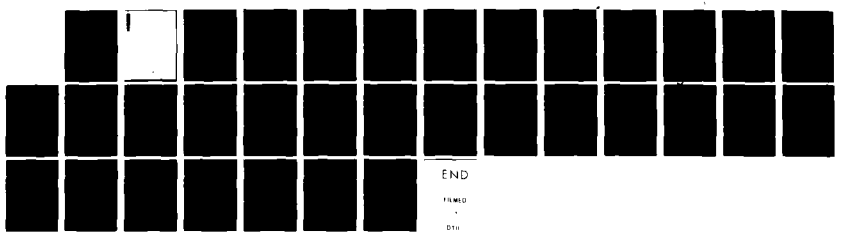

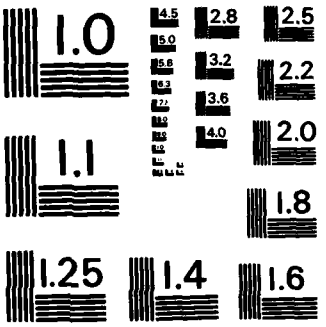

MICROCOPY RESOLUTION TEST CHART
NATIONAL BUREAU OF STANDARDS-1963-A

AD A121472

SECURITY CLASSIFICATION OF THIS PAGE (When Data Entered)

REPORT DOCUMENTATION PAGE	READ INSTRUCTIONS BEFORE COMPLETING FORM
1. REPORT NUMBER: NRL Memorandum Report 4948 AD-A121472	2. GOVT ACCESSION NO. / 3. RECIPIENT'S CATALOG NUMBER
4. TITLE (and Subtitle): CONSTRAINTS ON TRANSPORTABLE ION BEAM POWER	5. TYPE OF REPORT & PERIOD COVERED: Interim report on a continuing NRL problem.
	6. PERFORMING ORG. REPORT NUMBER
7. AUTHOR(s): P.F. Ottinger*, Shyke A. Goldstein* and D. Mosher	8. CONTRACT OR GRANT NUMBER(s)
9. PERFORMING ORGANIZATION NAME AND ADDRESS: Naval Research Laboratory, Washington, DC 20375	10. PROGRAM ELEMENT, PROJECT, TASK AREA & WORK UNIT NUMBERS: 47-0879-0-2
11. CONTROLLING OFFICE NAME AND ADDRESS: Department of Energy, Washington, DC 20545	12. REPORT DATE: November 12, 1982
	13. NUMBER OF PAGES: 32
14. MONITORING AGENCY NAME & ADDRESS (if different from Controlling Office)	15. SECURITY CLASS. (of this report): UNCLASSIFIED
	15a. DECLASSIFICATION/DOWNGRADING SCHEDULE

16. DISTRIBUTION STATEMENT (of this Report)

Approved for public release; distribution unlimited.

17. DISTRIBUTION STATEMENT (of the abstract entered in Block 20, if different from Report)

18. SUPPLEMENTARY NOTES

*Present address: JAYCOR, Inc., 205 S. Whiting Street, Alexandria, VA 22304

19. KEY WORDS (Continue on reverse side if necessary and identify by block number)

Intense ion beams
Transport
Stability
Energy loss
System study

ECTE
NOV 1 3 1982
A

20. ABSTRACT (Continue on reverse side if necessary and identify by block number)

Constraints on transportable high ion beam power are investigated in order to determine the number of modules required for a multi-modular light-ion ICF system. Electrostatic and electromagnetic stability constraints are examined as well as channel expansion and energy loss considerations. It is found that less than ten modules are required to drive a high gain pellet if large radius transport channels are used in conjunction with beam bunching and final focusing.

DD FORM 1 JAN 73 1473 EDITION OF 1 NOV 65 IS OBSOLETE
S/N 0102-014-6601

SECURITY CLASSIFICATION OF THIS PAGE (When Data Entered)

CONTENTS

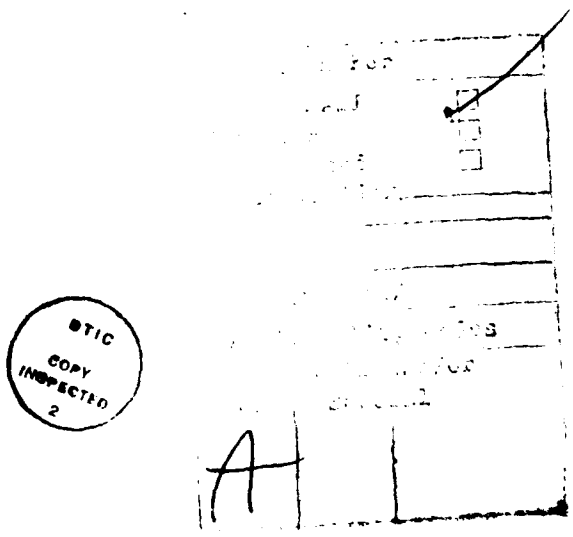

CONSTRAINTS ON TRANSPORTABLE ION BEAM POWER

1. INTRODUCTION

The development of terawatt-level ion beams has generated a great deal of interest in using light-ion beams to drive thermonuclear pellets.[1-9] Target design studies for light-ion beams indicate that ~4 MJ of ions must be delivered in ~10 ns to an ~1 cm diameter pellet in order to achieve high gain thermonuclear ignition.[10] Since present technology cannot provide a single-module pulsed-power system from which 4 MJ of ions can be extracted, a multimodule system is required. In addition, a transport scheme and a method for beam pulse compression are needed, since typical pulse durations are on the order of ~50 ns.

One possible transport scheme involves the use of a z-discharge channel for transporting ion beams.[11] Focusing can be achieved by a combination of geometric and magnetic-field focusing prior to injection into the channel.[12,13] Beam-pulse compression results from ramping the diode voltage so that the tail of the beam catches up to the head of the beam.[13,14] In addition, a final focusing cell can be used at the exit of the transport system to radially compress the beam to pellet size.[15] Figure 1 illustrates one module of such a multimodule system.

Assuming that the z-discharge channel is itself produced in the MHD stable configuration, the question of the effects that the passage of the beam will have on the equilibrium and stability of the beam-plasma system is an important one. The MHD response of the plasma has been treated elsewhere[16] and will only be briefly reviewed here. Analyses of stable beam propagation in straight and tapered channels, as well as in bumpy channels (subject to sausage instability), have also been done previously.[17] This work shows that,

Manuscript approved September 20, 1982.

in the absence of microinstabilities driven by the beam, good beam transport and bunching is possible under the conditions set by MHD considerations (which will be outlined in Sec. 3).[18] However, in the presence of microinstabilities, beam transport and bunching can be seriously affected.

Transport constraints arising from electrostatic (ES) and electromagnetic (EM) velocity-space instabilities,[19,23] which can grow on a time scale much faster than the beam pulse duration, will be reviewed in this report. The problem will be considered with the goal of identifying an operational window for good transport and bunching. The results will be presented in a general form so that they may be applied to beams of various low atomic number species propagating in channel plasmas of different compositions.

2. STABILITY CONSTRAINTS

In order to provide stable transport for the beam, certain constraints are put on the transport system. The two-stream instability will rapidly generate electrostatic microturbulence unless growth of the mode is prevented.[19,21,22] Such turbulence will degrade beam quality and confinement. By maintaining the plasma electron temperature below the critical temperature,

$$T_e^c(eV) = 10^{-5}\left(\frac{A_b^2\, n_p^3\, Z_p^5\, \lambda_{ei}^2}{Z_b^4\, n_b^2}\right)^{1/3}\left(\frac{\Delta V_z}{V_b}\right)^{4/3} , \qquad (1)$$

the two-stream mode will remain collisionally stabilized. In Eq. (1) A_b is the atomic weight of the beam ion, n_b and n_p are the beam and plasma ion densities measured in particles/cm^3, Z_b and Z_p are the beam and plasma ion charge states, V_b is the beam velocity, ΔV_z in the axial velocity spread of the beam and λ_{ei} is the Coulomb logarithm. In general, the most severe

constraint on T_e exists at the tail of the beam (after the front of the beam has heated the channel) prior to beam bunching (at the beginning of the transport channel). Note that by increasing n_p, T_e^c can be raised. Operating at twice the density required for minimum beam energy loss during transport, increases T_e^c by a factor of two but only increases the beam energy loss by 25%.[16]

One can estimate the final temperature from the rate of collisional beam deposition in the channel plasma by using[16]

$$T_e^f \text{ (eV)} = T_0 + 6.9\times10^9 J_b \tau_b / \bar{E} \quad , \tag{2}$$

so that the ES stability constraint is given by

$$T_e^f < T_e^c \quad . \tag{3}$$

Here T_0 is the initial electron temperature measured in eV, J_b is the beam current density measured in MA/cm^2, τ_b is the pulse duration of the beam measured in seconds and $\bar{E}$ is the average beam energy measured in MeV. In deriving Eq. (2) it is assumed that $T_e \sim T_i$ since this is the usual case; this also precludes the existence of ion acoustic instability. In plotting constraint curves one-to-two times the density required for minimum beam energy loss is used to calculate n_p and a 10% spread in beam energy is assumed so that $\Delta V_z/V_b = 0.05$ in Eq. (1). T_0 was chosen to be ~10 eV in Eq. (2). It will also be assumed in all the stability constraints considerations that

deuterium gas is used to fill the transport system so that Z_p=1 and A_p=2. If the beam is monoenergetic, $\Delta V_z/V_b \sim \theta_m^2$ for the ES stability constraint. Here θ_m is the maximum angle of injection into the transport channel. However, foil scattering and field fluctuations are expected to produce a spread in beam ion energies of about 10% and this spread will be used in the ES stability constraint curves. Energy spreads larger than about 15% at injection into the channel may adversely affect beam bunching.

Growth of electromagnetic waves can be held to a tolerable level by allowing for a reasonable spread in beam perpendicular energy and limiting the beam current density.[20-23] If the beam is too cold, beam filamentation can occur during transport. The condition for good beam transport is

$$\theta_m^2 \sim \frac{V_\phi^2}{V_b^2} > 3.2\times10^{-18}\left(\frac{Z_p \lambda_{ei} n_b \tau_b}{A_b T_e^f T_o^{1/2}}\right) , \qquad (4)$$

where V_ϕ is a measure of azimuthal velocity spread in the beam and T_e^f and T_o are defined in Eq.(2). Here it is assumed that the azimuthal velocity spread is comparable with the radial velocity spread (i.e., $\theta_m \sim V_\phi/V_b$), which is consistent with experimental observations. Note that high electron temperatures are beneficial here, whereas $T_e^f < T_e^c$ is required for two-stream stability.

If the beam does not filament but the beam current density is too high, the return current in the channel can cause channel filamentation. In order to prevent this from occurring requires that[22]

$$J_b \leq 3.6\times10^{-18}(A_p n_p)^{1/2}\left[(2-Z_p^{-1})t_1+\frac{1}{n_p Z_p^{3/2}}\frac{.1\times10^{18}J_b\tau_b A_p}{T_e}^{1/2}\left(T_e^{f\,1/2}-[T_o+(T_e^f-T_o)\frac{t_1}{\tau_b}]^{1/2}\right)\right]^{-1}, \quad (5)$$

where t_1 is defined as the time it takes for the beam to heat the plasma to $T_e(t_1) = 1.4\times10^{-4}(Z_p^3 n_p \lambda_{ie}^2)^{1/4}$ in eV. If $T_e(t_1)<T_o$, $t_1=0$ and the first term in the large square brackets on the right hand side of Eq. (5) is dropped. If $t_1>\tau_b$ the last term in the large square brackets is dropped. In the cases considered in Sec. 4, the first term in the square brackets in Eq. (5) can be ignored, since T_o is found to be ~ 10 eV for deuterium discharges which is typically greater than $T_e(t_1)$. For higher Z channel gases this may not be the case.

Eqs. (3)-(5) are the stability constraints which limit the transportable beam power. These constraints along with MHD and energy-loss considerations will determine an operational window for good transport and bunching.

3. MHD AND ENERGY-LOSS CONSTRAINTS

The plasma return current driven in the channel during beam transport results in a radial $\underset{\sim}{J}x\underset{\sim}{B}$ driven expansion of the channel plasma.[16] Typically, thermal expansion is unimportant. In order to avoid excessive channel expansion, the beam current is limited to

$$I_b \leq 3\times10^{-10}\,\rho\, r_{ch}^4/\tau_b^2\, I_{ch}\,, \quad (6)$$

where I_b and I_{ch} are the beam and channel current in MA, ρ is the mass density of the channel in g/cm^3 and r_{ch} is the channel radius in cm. Here it is assumed that the beam radius r_b, is equal to r_{ch}. The uniform channel current inside r_{ch} required to confine the beam can be expressed as[17]

$$I_{ch} = 1.3\,\theta_m^2\, A_b^{1/2}\, \bar{E}^{1/2}/Z_b\,, \quad (7)$$

where $\bar{E}$ is the beam particle energy in MeV. The strong dependence of I_b on r_{ch} makes large radius transport very attractive, however, a final focusing scheme must then be employed to radially compress the beam to pellet size after transport. A factor of three compression in radius seems easily attainable in the final focusing cell and will be assumed for many of the plots in Sec. 4.

The transport channel length is determined by bunching requirements and is given by[18]

$$L = 1.3\times10^9 \left(1-\frac{1}{\alpha}\right) (\tau_t-\tau_b)\, E(\tau_b)^{1/2}/A_b^{1/2}, \qquad (8)$$

where $E(\tau_b)$ is the final ion energy produced at the end of the pulse, α is the bunching factor and τ_t is the transit time of the beam from the diode exit to the bunching location. The transit time is also related to the diode voltage ramp with

$$\phi(t) = \phi(0)/(1-t/\tau_t)^2 \quad , \qquad (9)$$

where $\phi(t)$ is the ideal diode voltage waveform. Here it will be assumed that a factor of 5 bunching is acheived with a beam energy spread at the bunching location of 50%, so that

$$L = 4\times10^9\, \tau_b\, \bar{E}^{1/2}/A_b^{1/2} \quad , \qquad (10)$$

where now L is written in terms of the average ion energy, $\bar{E} = [E(0)+E(\tau_b)]/2$. With the assumption of a 50% energy spread at the bunching location, one finds $E(0) = 3\bar{E}/4$ and $E(\tau_0) = 5\bar{E}/4$. This channel length then determines the beam energy lost during transport. It is also assumed that the focusing distance, F, is much shorter than L so that the bunching length and channel length are approximately equal.

The beam losses energy to the channel plasma by collisional slowing down and deceleration in the self-consistent axial electric field generated in the plasma. The electric field results from a resistive J_p/σ component and an inductive $\underline{V}_p x \underline{B}$ component with the latter typically larger. Assuming that the electric field is predominately inductive, the optimum mass density for the channel for minimum energy loss during transport is given by[16,18]

$$\rho_{opt} = 0.167 \frac{\bar{E} I_b^{1/2} \tau_b^{1/2} \theta_m^2}{r_b^2 Z_b^{3/2}} \tag{11}$$

For $\rho = x\rho_{opt}$ and deuterium as the fill gas in the channel, the fraction of beam energy lost during transport over the distance L (defined in Eq.(10)) is expressed as

$$\frac{\delta E}{\bar{E}} = 6.7 \times 10^{11} \left(x + \frac{1}{x}\right) \frac{\theta_m^2}{r_b^2} \left(\frac{A_b Z_b I_b \tau_b^3}{\bar{E}}\right)^{1/2} \tag{12}$$

Because Eq. (12) was derived for ions with the average energy, ions at the head of the beam will lose slightly more energy and ions at the tail of the beam will lose slightly less energy. Also, since $\delta E/\bar{E}$ as a function of x has a minimum at x=1, variations of x about x=1 will not change $\delta E/\bar{E}$ dramatically. Operating at twice the optimum mass density, or at x=2, only changes $\delta E/\bar{E}$ by 25% but considerably relieves the stability constraints as will be observed in Sec. 4.

The MHD and energy-loss constraints are then given by Eqs. (6) and (12) when combined with the stability constraints found in Sec. 2, the operational window for good beam transport and bunching is defined.

4. OPERATIONAL TRANSPORT WINDOW

The operational window is defined by the constraints on the transport system derived from ES stability conditions (Eq. (3)), beam and channel filamentation considerations (Eqs. (4) and (5)), MHD considerations (Eq. (6)) and beam energy-loss limitations (Eq. (12)). All constraints are written in terms of the average ion energy $\bar{E}=[E(0)+E(\tau_b)]/2$. Constraints at the head of the beam will be slightly more restrictive while those at the tail of the beam will be slightly more relaxed. For each of these five constraints, a condition on the transportable beam power can be derived as a function of the angular spread in the beam measured by θ_m. For convenience, the conditions will be expressed in terms of $E_o=\bar{E}/A_b^{1/2}Z_b$ which is the energy of an equivalent-range proton. In terms of E_o the beam power can be written as $P=I_b A_b^{1/2} E_o$ where P is in TW, I_b is in MA and E_o is in MeV. It will also be assumed that the channel gas is deuterium. Otherwise, the simple estimate for T_e^f given in Eq. (2) must be replaced by a much more complicated expression because of the more complex chemistry and radiation processes in higher atomic number gases.

The conditions on the transportable beam power will be expressed as functions of R/F where $R/F=\theta_m$ when the beam is focused a distance F downstream from a diode of radius R.[12,18] The transport channel entrance is positioned at the focus and the maximum injection angle into the channel is R/F. This assumes that R/F is much larger than the angular divergence of the beam at the source. If this is not the case, or if a small radius diode is used with no focusing, then P should be plotted as a function of θ_m, the angular divergence of the beam at the channel entrance. In that case, the horizonal axis in the plots should read θ_m rather than R/F and R/F should be replaced by θ_m in Eqs. (13)-(17).

Each of the five conditions on P(R/F) will depend only on the parameters x, E_o, r_b, τ_b, A_b and Z_b. In all that follows it is assumed that $r_{ch} = r_b$, $\rho = x\rho_{opt}$, $\alpha = 5$, $\Delta E/\bar{E}$ before bunching ~ 0.1, $\Delta E/\bar{E}$ after bunching ~ 0.5 and the pellet radius is ~ 0.5 cm. In deriving the constraints due to filamentation considerations, it is assumed that $T_e(t_1) < T_o < 10$ eV so that the first term in Eq. (5) can be dropped. The five conditions are then:

i) ES stability condition before bunching.

$$P < P_{ES} \equiv 1.6\times10^{-3}\left(\frac{x^6 r_b^8 A_b^{13/2}\lambda_{ei}^4 R^{12}}{Z_b^5 \tau_b^3 F^{12}}\right)^{1/7} E_o^3 \quad , \tag{13}$$

where

$$\lambda_{ei} = 24 - \ln\left[\frac{10^2 R\, r_b}{F}\left(\frac{E_o^9 A_b^{1/2} x^2}{Z_b \rho^3 \tau_b^3}\right)^{1/4}\right] \quad ,$$

and 1.6×10^{-3} is replaced in Eq. (13) by 1×10^{-2} to obtain the ES stability condition after bunching occurs in order to reflect the increased velocity spread in the beam;

ii) beam filamentation condition

$$R/F > \theta_{BF} \equiv 2.5\times10^{-2}\left(\frac{\lambda_{ei}^4 E_o^2}{A_b^5 Z_b^6}\right)^{1/8} \quad , \tag{14}$$

where P only enters weakly through λ_{ei} ;

iii) channel filamentation condition

$$P < P_{CF} \equiv (1.76\times10^5 x^2 R^4/Z_b F^4)\ (E_o^{14}\tau_b^2 A_b^{11})^{1/6}; \tag{15}$$

iv) MHD channel expansion condition

$$P < P_{MHD} \equiv 1.5\times10^{-21} x^2 r_b^4 E_o^2/\tau_b^3 \ ; \tag{16}$$

and

v) beam energy-loss condition

$$P < P_{\delta E} \equiv \frac{1.36\times10^{-25} r_b^4 E_o^2 F^4}{(x+x^{-1})^2\ \tau_b^3 R^4} \ , \tag{17}$$

where it is assumed that $\delta E/\overline{E} < 0.25$. In general, the beam ions are fully stripped after passing through the cathode foil, which separates the diode vacuum regime from the gas filled focusing region, and the foil between focusing region and the transport channel.

In the plots that follow, the operational window is defined by the shaded region with the boundaries of the window defined by Eqs. (13)-(17). The two left boundaries are the beam and channel filamentation constraints (ii and iii), the top boundary is the ES stability condition (i) and the right boundary is the energy-loss limitation constraint (v). The MHD-channel-expansion condition (iv) is easily satisfied in all the cases that will be considered and will not play a role in defining the operational windows. In some cases, the channel-filamentation constraints (iii) will be severe enough to dominate over the beam filamentation constraints (ii) or the ES stability condition (i) or both so that the window has only three (e.g., Fig. 5) or two (e.g., Fig. 6) boundaries rather than four.

For a given beam-energy spread and energy-loss limitation, the top and right boundaries are hard boundaries whereas the beam and channel filamentation constraints on the left boundary are somewhat fuzzy. The

filamentation constraints are derived by assuming that less than one e-fold occurs during beam transport but the initial perturbation level is unknown. If the initial perturbation is small, then the filamentation constraints given in Eqs. (14) and (15) are too severe and the left boundaries can be moved further to the left. Channel hydromotion and time variations in the beam distribution function will also tend to relax the filamentation constraints.

The dashed line in the window is the ES stability constraint if the beam were monoenergetic. A beam energy spread of 10%, as assumed in Eq. (13), considerably increases the size of the operational window by moving the ES stability constraint up to the top boundary.

The contours in the plots are lines of constant density. In each plot for a given P and R/F the channel density is defined by $n_p = x\rho_{opt}/2M$ where 2M is the mass of a deuteron and ρ_{opt} is defined in Eq. (11). The upper set of numbers labeling the contours denotes the ion density of the plasma in units of 10^{17} particles/cm^3. The lower set of number in parenthesis is the percentage of the beam energy which is lost during transport at the specified plasma density. The required channel current (Eq. (7)) and the final electron temperature (Eq. (2)) for a given P and R/F can also be determined from each plot by referring to the scale either above or to the right of the plot. The quantity I_{ch} is independent of P and T_e^f is independent of R/F.

In Figs. (2)-(5) the operational window is shown for H^{+1}, D^{+1}, He^{+2} and C^{+6} respectively for E_o=2 MeV, x=1, r_b=0.5 cm and $\tau_b=5\times10^{-8}$s. The size of the window increases with increasing atomic number. Table 1 shows that three of the five constraints are relaxed by increasing A_b while the other two are unchanged. This results from the fact that less beam current is required to transport the same beam power at the same E_o as A_b is increased. Higher A_b

allows transport of both higher power and lower R/F beams, so that the transportable beam power brightness $P/(R/F)^2$, improves considerably.

By increasing x (i.e., the channel plasma density), the ES stability, channel filamentation and channel expansion constraints are relaxed but the beam energy-loss constraint is more severe. Because the beam energy-loss constraint is being varied about a minimum, the change in this constraint is not dramatic. This is shown in Fig. 6 which should be compared with Fig. 2. The real benefit of increasing x is not realized unless r_b and/or E_0 are simultaneously increased in order to relax the energy-loss constraint. This will be shown more clearly in Fig. 9.

In Fig. 7 the parameters are all the same as in Fig. 2 except that the channel and beam radii are increased from 0.5 cm to 1.5 cm. The ES stability channel expansion and beam energy-loss constraints are all relaxed while the filamentation constraints are unchanged. The operational window has increased considerably in size with a maximum transportable power now on the order of 5 TW at R/F of about 0.18 radians. This results from decreasing the beam power density by spreading the beam over an area 9 times larger than in the case considered in Fig. 2. In order to bring R/F to a lower value and improve beam brightness, x and/or E_0 must be increased at the same time as r_b (see Fig. 9) so that the channel filamentation constraint is reduced.

By increasing E_0 all the constraints are relaxed with the exception of the beam filamentation constraint which becomes more severe. This is shown in Fig. 8 where all the parameters are the same as Fig. 2 except that E_0 is increased from 2 MeV to 4 MeV. The maximum transportable power in this case is about 2.8 TW. The increased beam stiffness and lower beam current for a given power level allows higher power transport, however, lower electron temperatures allows the beam filamentation instability to grow at higher R/F

values than in Fig. 2. This is a result of reduced stopping power of the plasma for higher energy beams.

The combination of increased x, r_b and E_o, as evaluated in Fig. 9, improves the transportable power considerably to a peak of about 40 TW at about 0.14 radians for protons. These results should be compared with Fig. 2. At 25 TW the operational transport window has a width in R/F from 0.11 to 0.16 radians. Similar results for D^{+1}, H_e^{+2} and C^{+6} are shown in Figs. 10-12. Once the beam bunches down to a pulse duration of 10 ns, the operational window opens even further as seen in Fig. 13. From Table 1 it can be seen that the ES stability, channel expansion and beam energy-loss constraints all are relaxed when τ_b is decreased. Only the channel filamentation constraint is more severe due to the low plasma temperature attained during the shorter pulse duration. Thus it is possible to transport the high power levels obtained after beam bunching.

5. CONCLUSIONS

By transporting in large-radius channels and ramping the diode-voltage waveforms to take advantage of time-of-flight bunching, high-power, light-ion beams can be delivered to a target a few meters from the diode. The radius of the channel is limited by the ability to compress the beam radially in a short, final-focusing cell positioned at the end of the transport system. Operating at a channel density which is slightly higher than ρ_{opt} and at an ion energy which is close to the high end of the acceptable energy range (defined by target designs) considerably increases the operational transport window for a large radius beam. For r_b = 1.5 cm, x = 2 and 4 MeV protons, it has been shown that a 40 TW beam can be transported with an angular divergence of about 0.14 radians (see Fig. 9). For higher atomic weight beams, such as D^+, He^{+2} and C^{+6}, even higher power levels can be successfully transported

(see Figs. 10-12). The availability of relatively pure source of higher atomic weight ions is still in question. If lighter, faster moving impurities are generated in sufficient quantities in a higher-atomic-weight ion beam, damaging preheat of the pellet may occur.

Although a pulse compression of $\alpha = 5$ was assumed, the actual power multiplication will be less. Comparing the power after bunching $(\alpha/\tau_b) \int_0^{\tau_b} P(t)dt$, with the power at the average energy ($\bar{E}$, as used in Figs. 2-12), one finds a power multiplication of about 4.8. Thus, when comparing the power level before bunching in Fig. 9 with the power level after bunching in Fig. 13, a power multiplication of 4.8 should be used rather than 5. If the figures had been plotted at $E(\tau_b)$, comparison of peak powers before and after bunching would result in a power multiplication factor of only 3.1. In all of these calculations it is assumed that the 10 ns power pulse after bunching is flat topped and that $I \sim E$ at high diode voltages.

From Fig. 13 one finds that propagating a 100 TW, 10 ns beam is feasible at R/F = 0.15 radians. This corresponds to about a 20 TW, 50 ns beam before bunching which is easily within the operational window given in Fig. 2. In order to deliver 4 MJ to a pellet in 10 ns, only 4 channels are required. Thus, if time-of-flight bunching of the beam and final focusing can be demonstrated, transport of beams at power levels sufficient to ignite a pellet should be possible in less than 10 and possibly in as few as 4 channels.

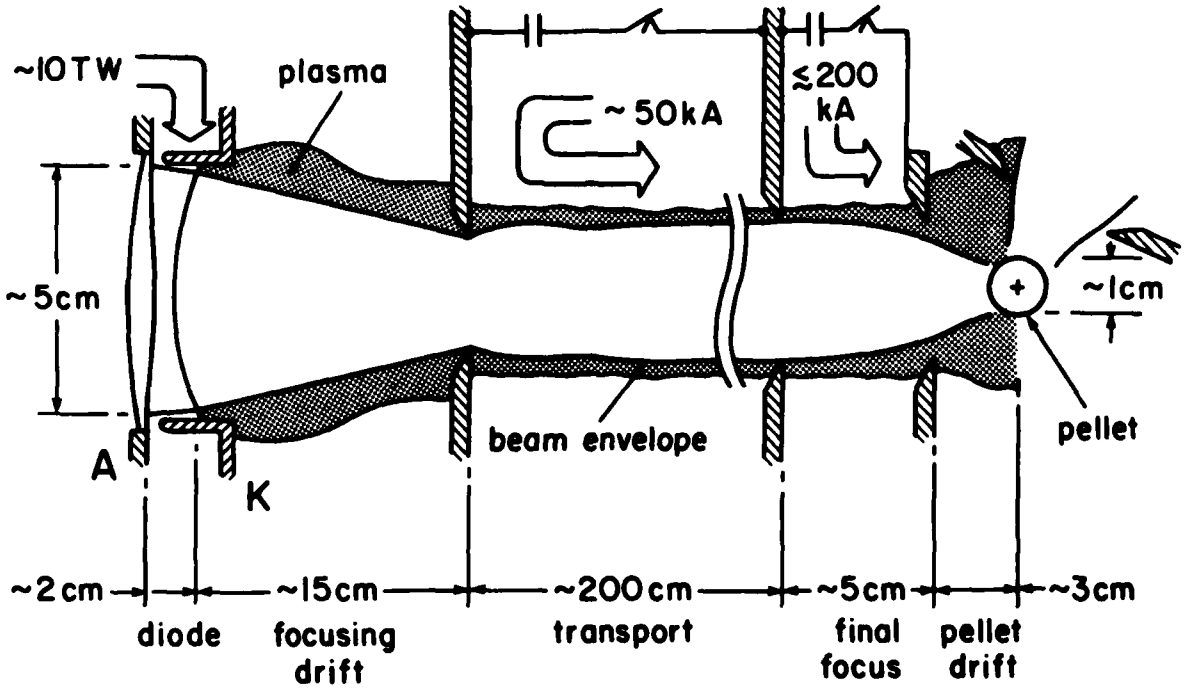

Figure 1 - Schematic of one module of a multimodule light-ion ICF system.

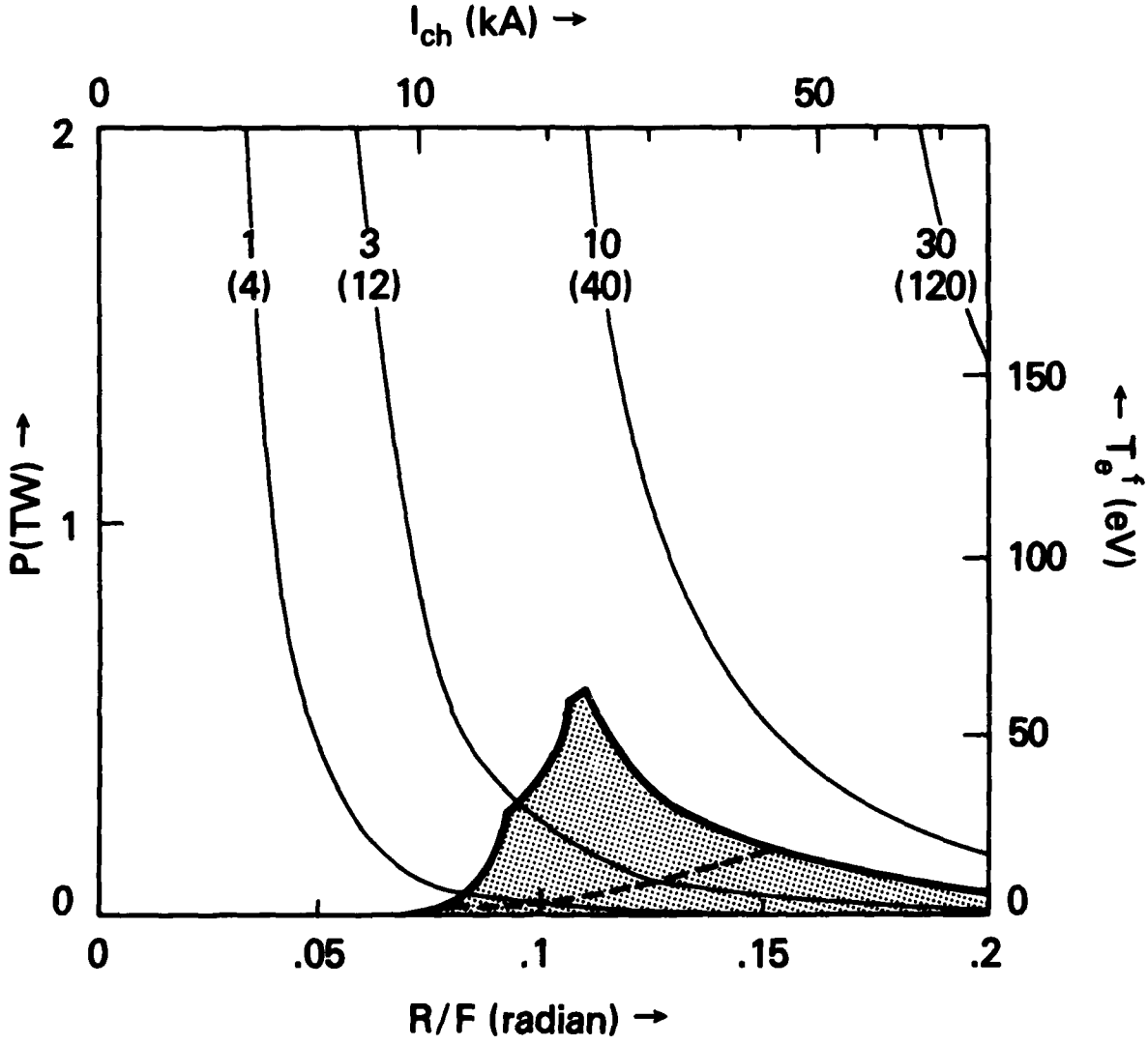

Figure 2 - Operational transport window for a H^{+1} beam with x = 1, r_b = 0.5 cm, E_o = 2 MeV and τ_b = 5×10^{-8} s.

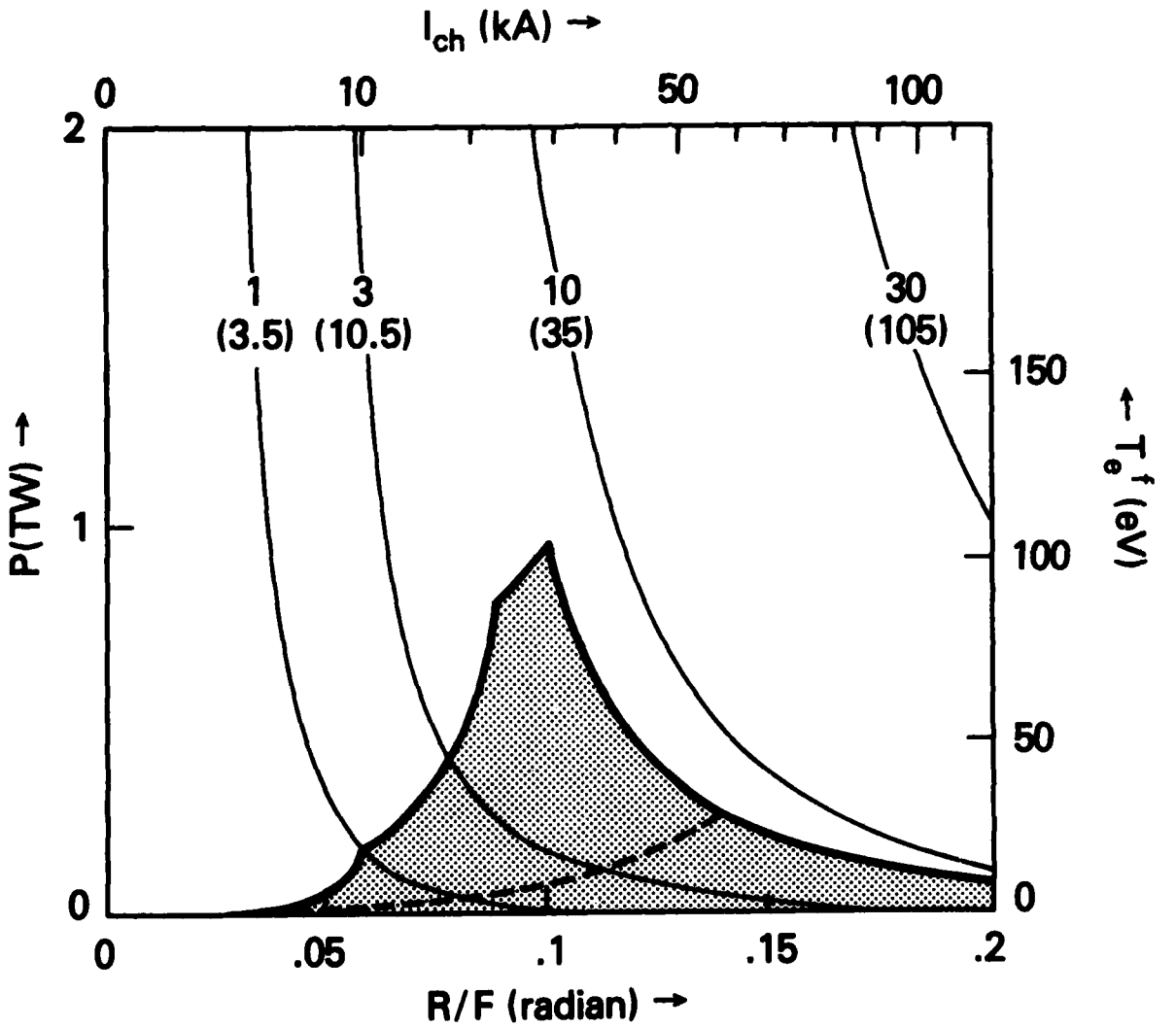

Figure 3 - Operational transport window for a D^{+1} beam with x = 1, r_b = 0.5 cm, E_o = 2 Mev and τ_b = 5×10^{-8} s.

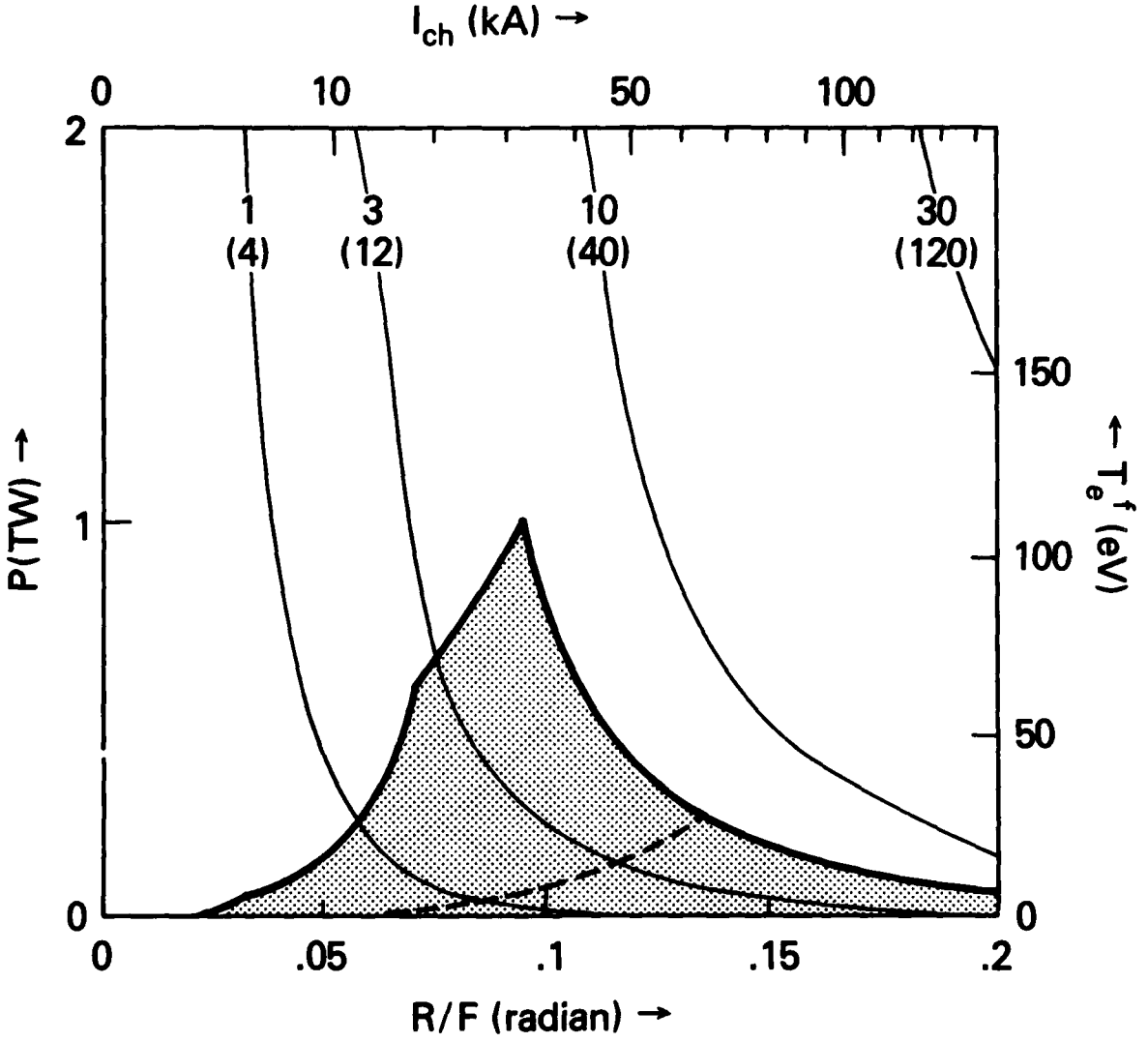

Figure 4 - Operational transport window for a He^{+2} beam with x = 1, r_b = 0.5 cm, E_o = 2 MeV and τ_b = 5×10^{-8} s.

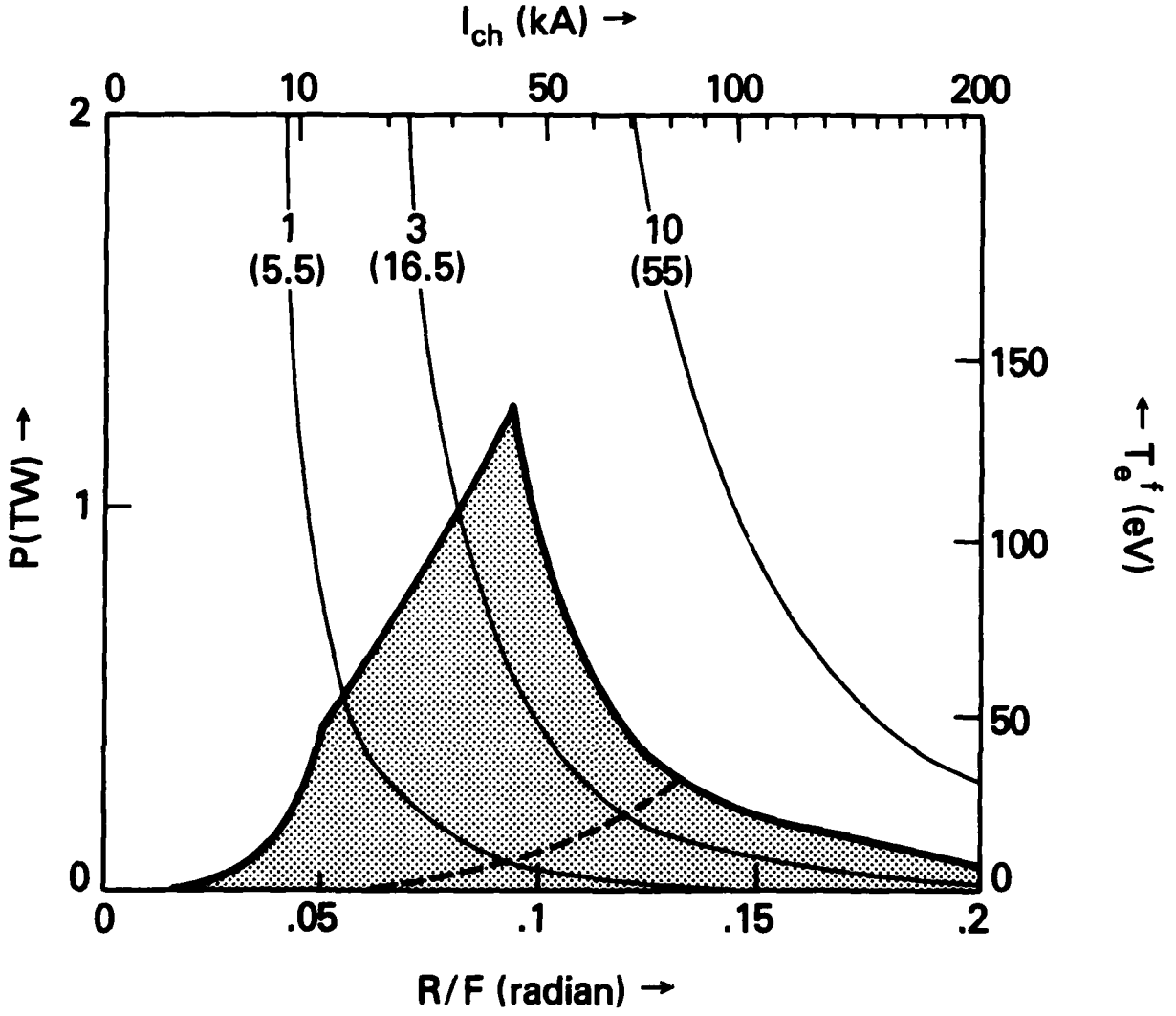

Figure 5 - Operational transport window for a C^{+6} beam with x = 1, r_b = 0.5 cm, E_o = 2 MeV and τ_b = 5×10^{-8} s.

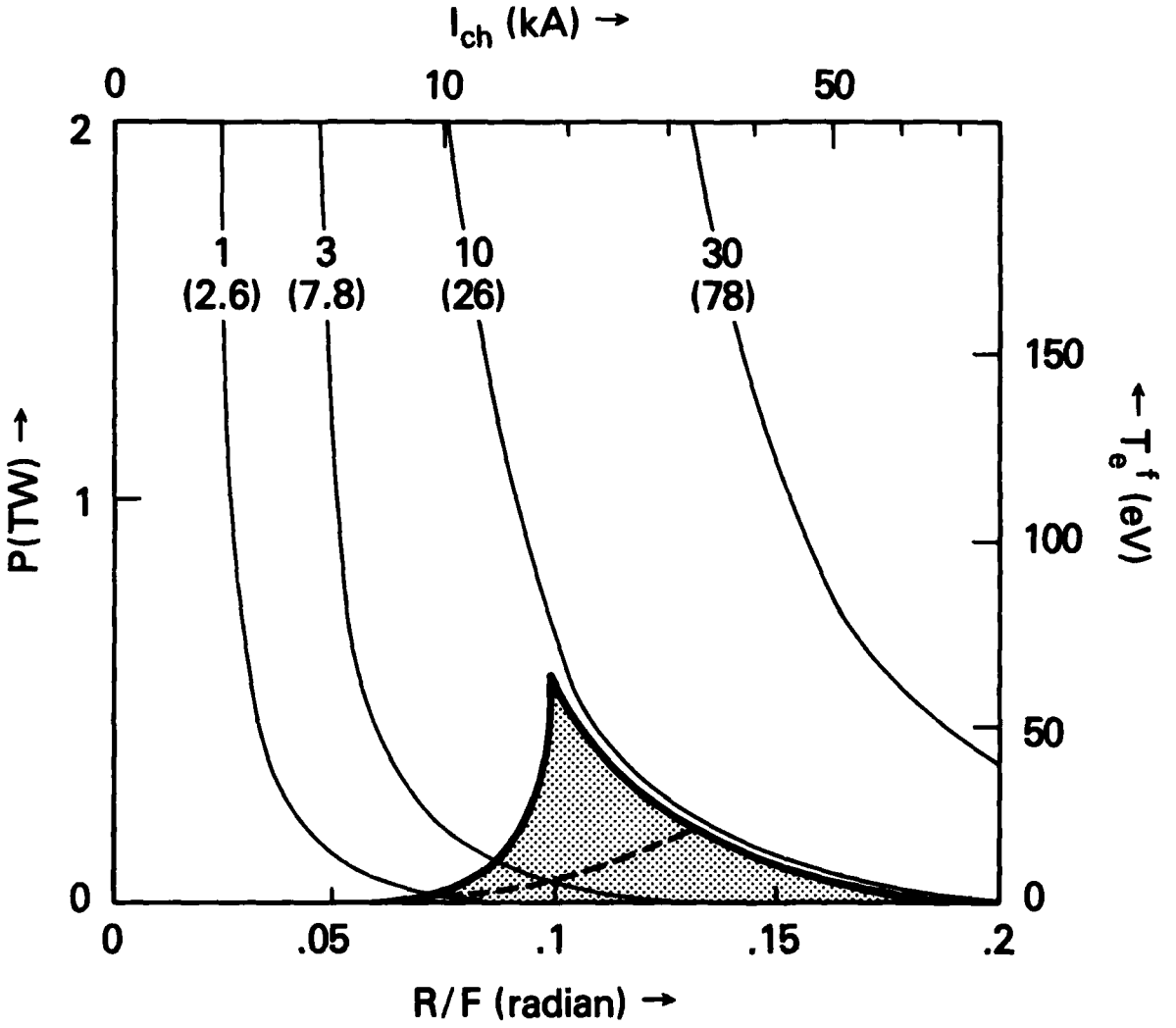

Figure 6 - Operational transport window for a H^{+1} beam with x = 2, r_b = 0.5 cm, E_o = 2 MeV and τ_b = 5×10^{-8} s.

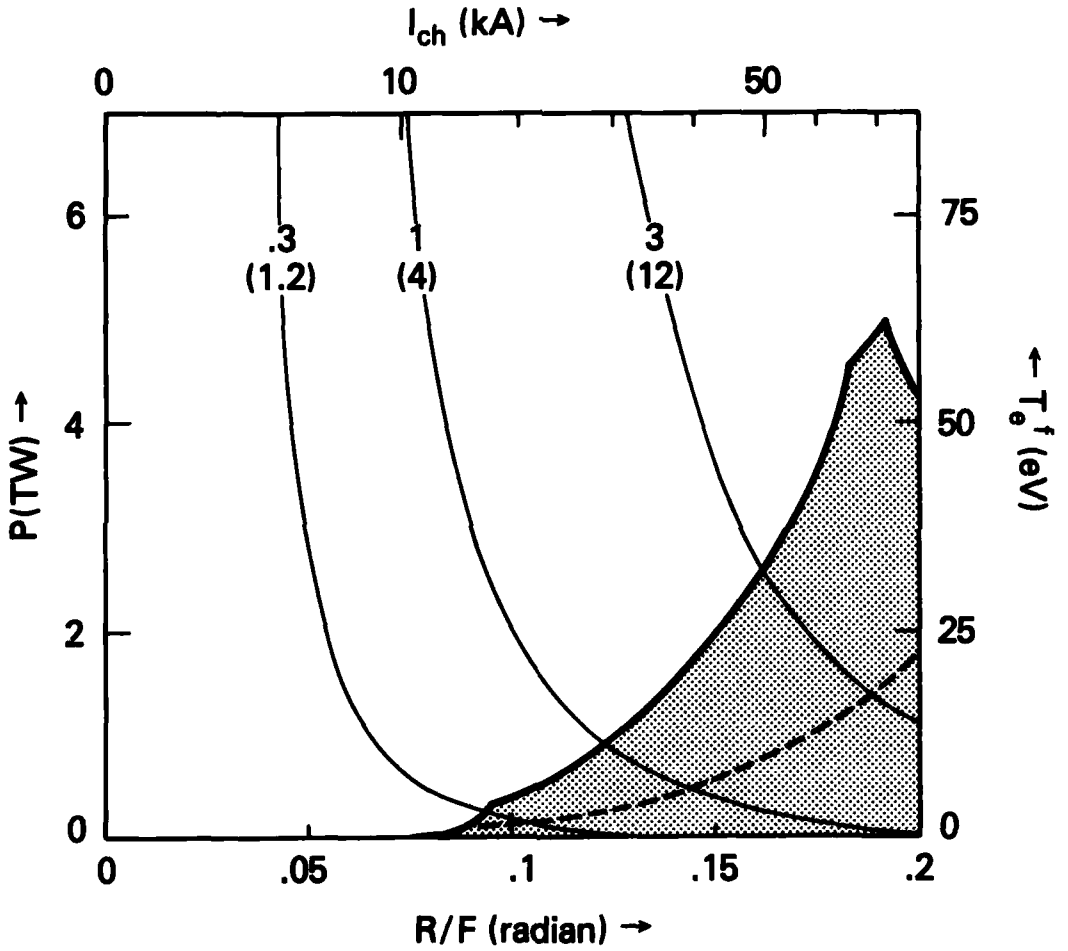

Figure 7 - Operational transport window for a H^{+1} beam with x = 1, r_b = 1.5 cm, E_o = 2 MeV and τ_b = 5×10^{-8} s.

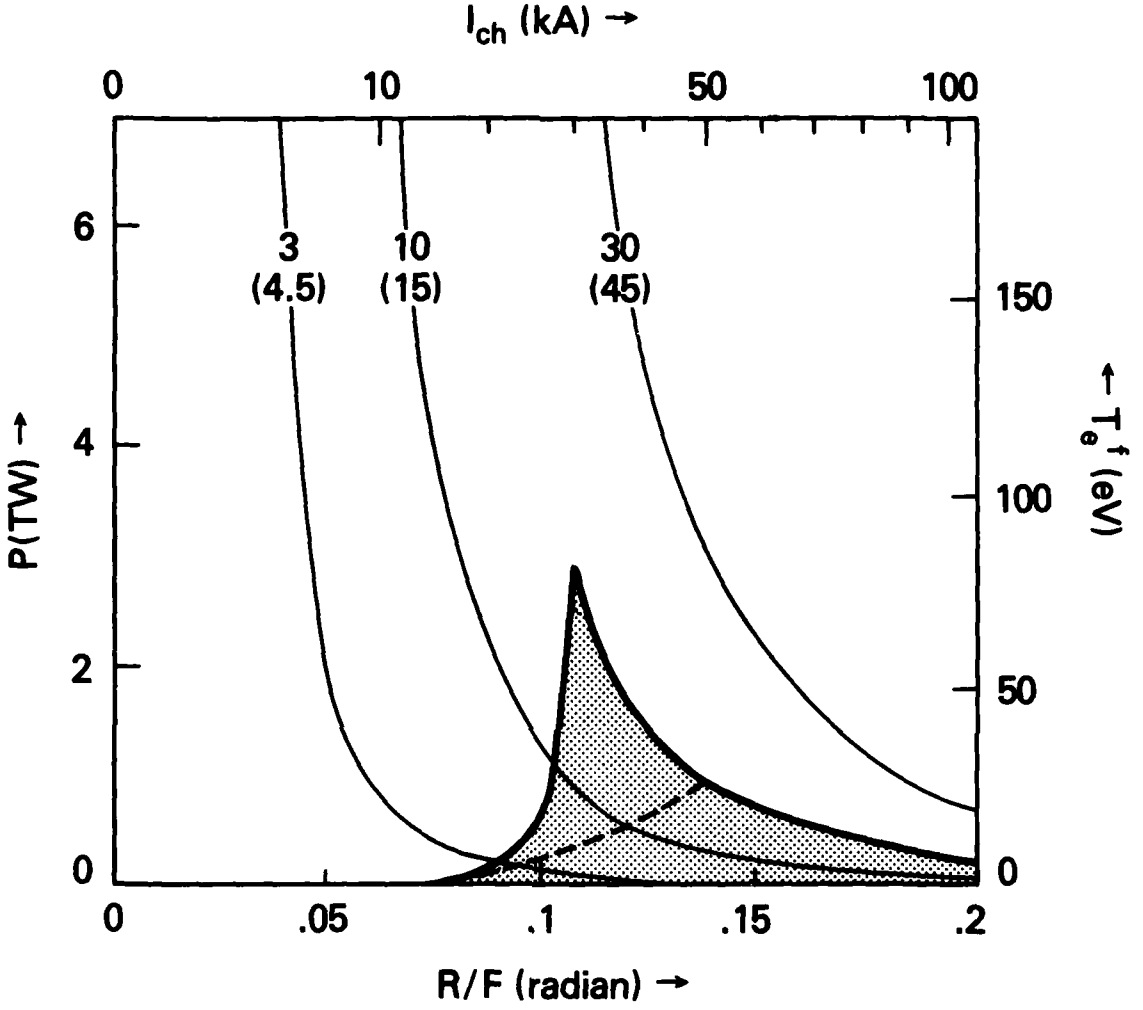

Figure 8 - Operational transport window for a H^{+1} beam with x = 1, r_b = 0.5 cm, E_o = 4 MeV and τ_b = 5×10^{-8} s.

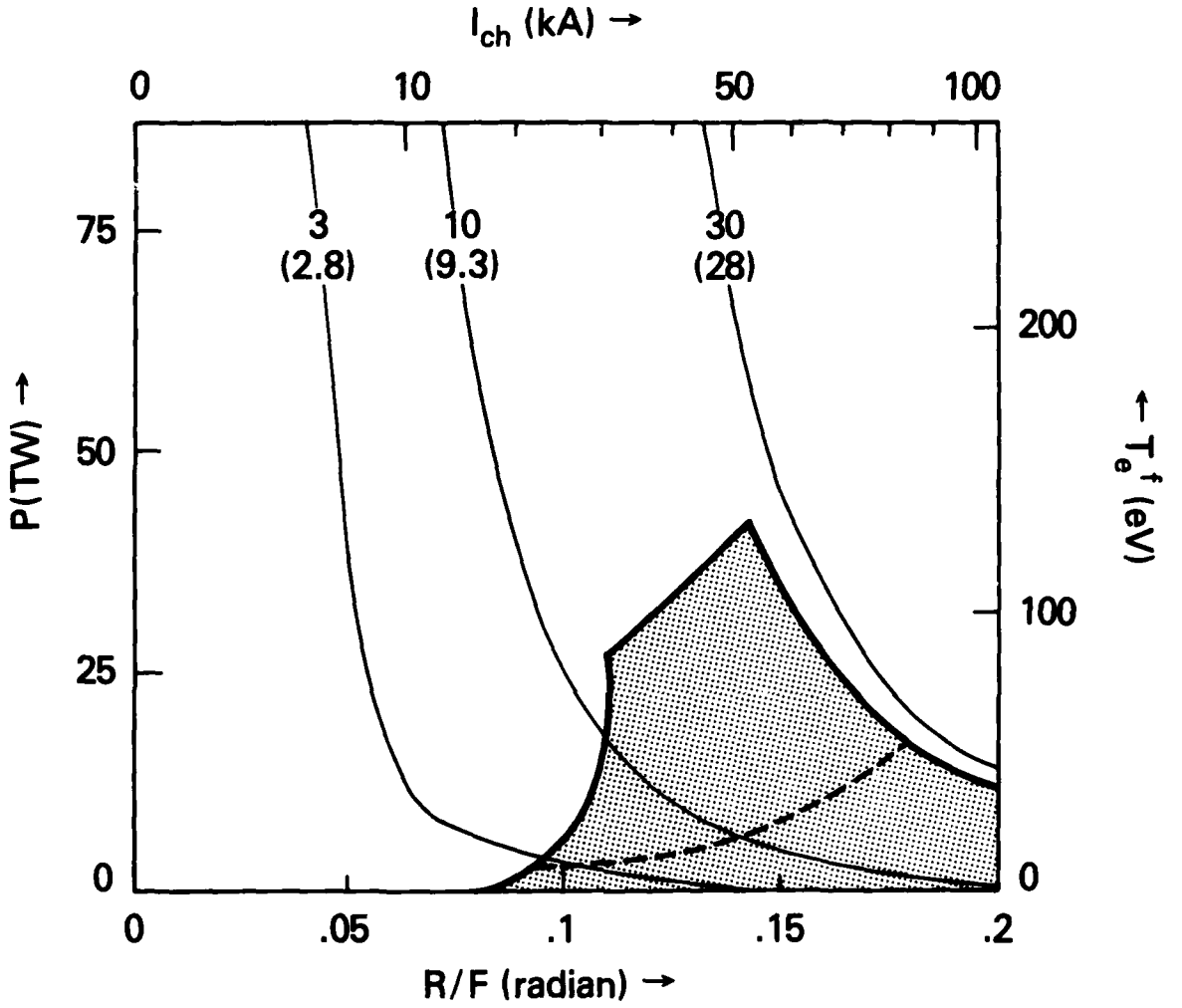

Figure 9 - Operational transport window for a H^{+1} beam with x = 2, r_b = 1.5 cm, E_o = 4 MeV and τ_b = 5×10^{-8} s.

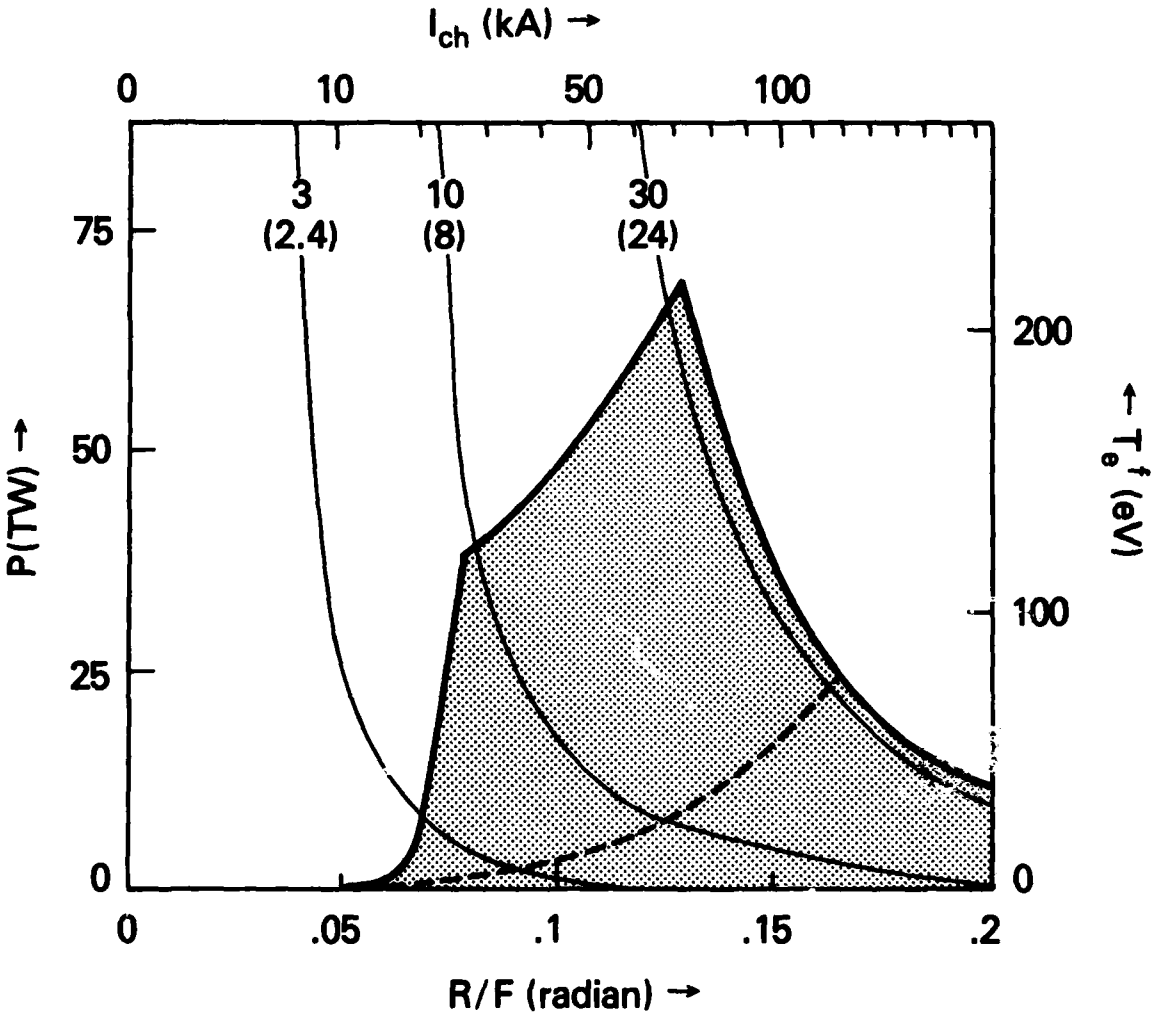

Figure 10 - Operational transport window for a D^{+1} beam with x = 2, r_b = 1.5 cm, E_o = 4 MeV and τ_b = 5×10^{-8} s.

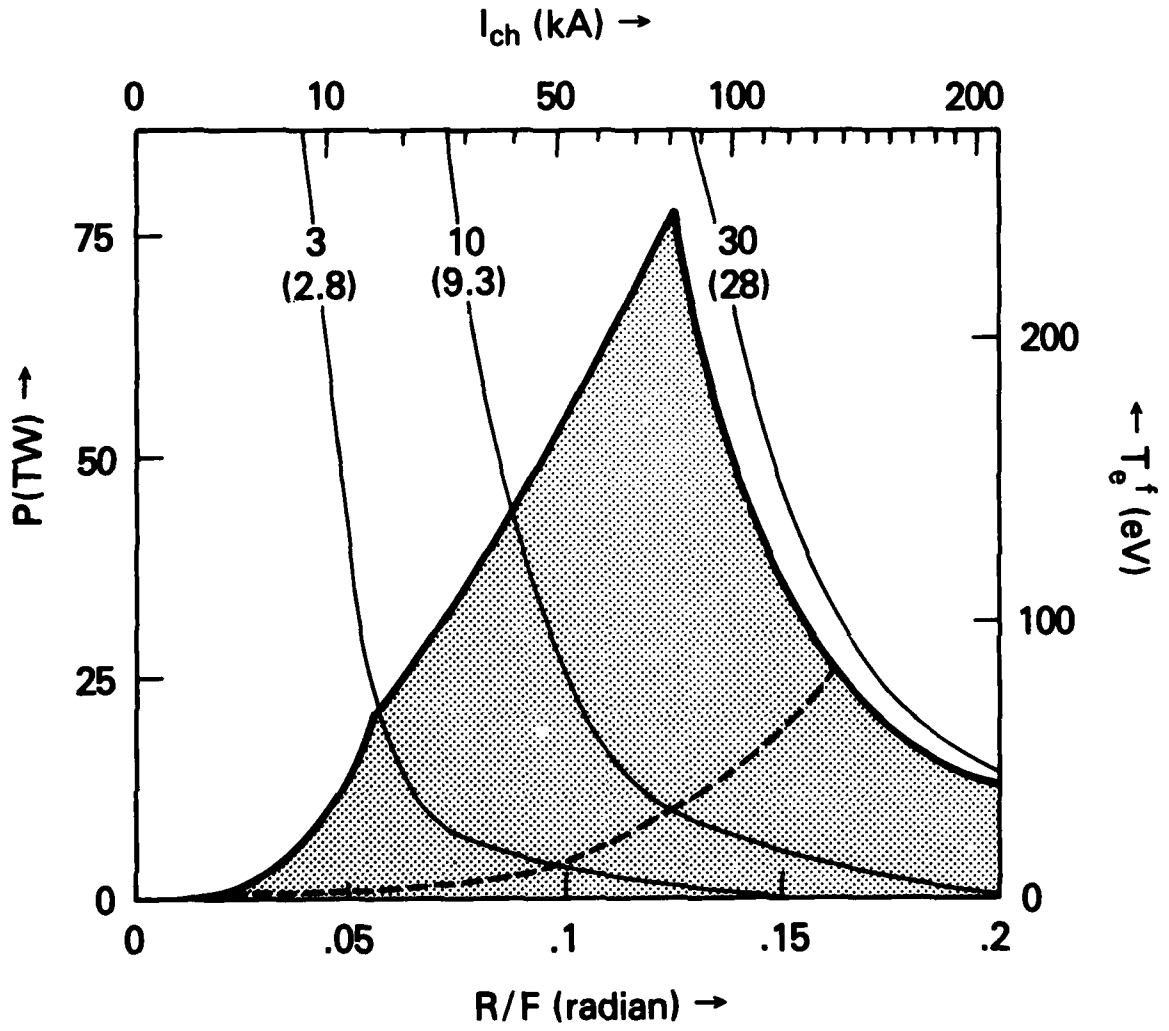

Figure 11 - Operational transport window for a He^{+2} beam with x = 2, r_b = 1.5 cm, E_o = 4 MeV and τ_b = 5×10^{-8} s.

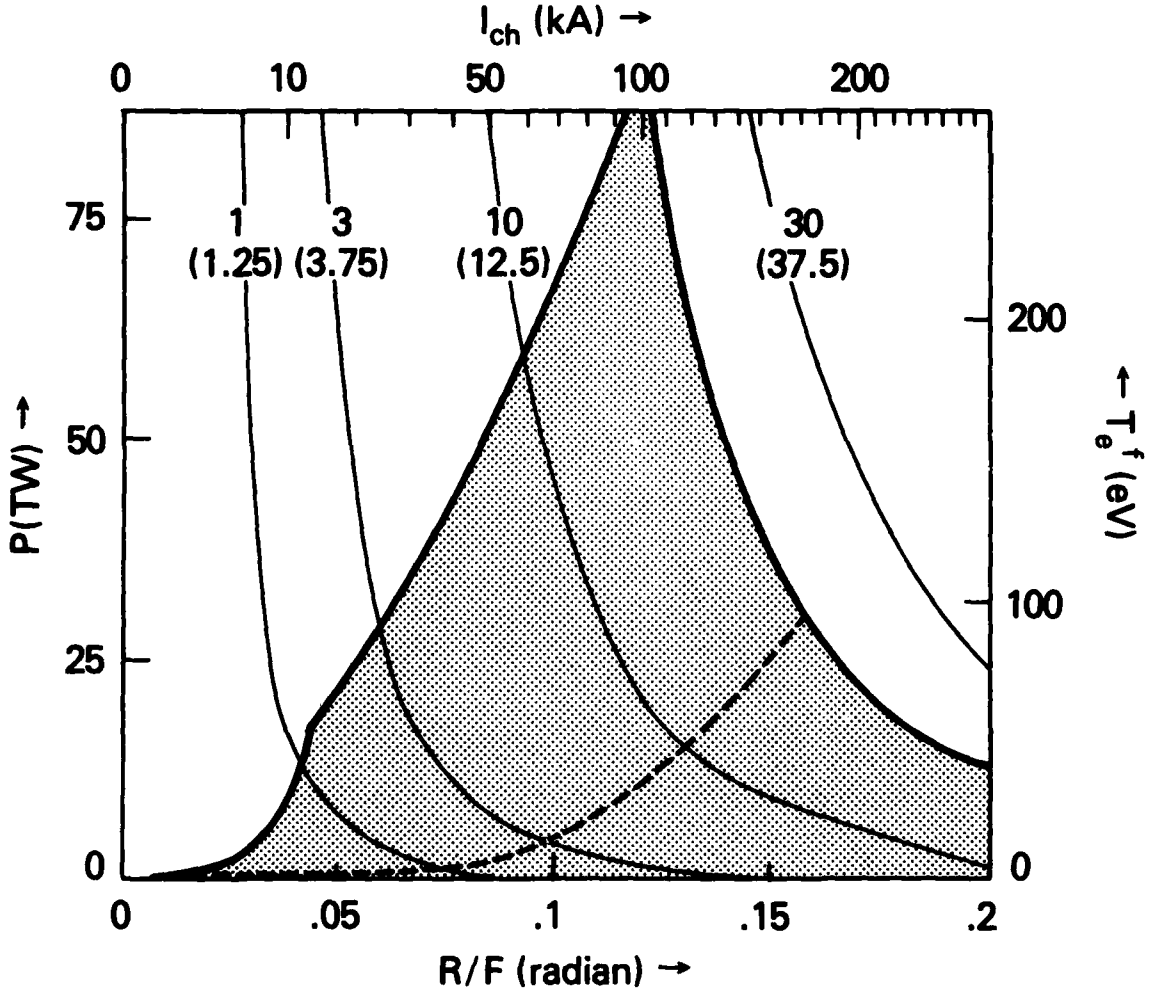

Figure 12 - Operational transport window for a C^{+6} beam with x = 2, r_b = 1.5 cm, E_o = 4 MeV and τ_b = 5×10^{-8} s.

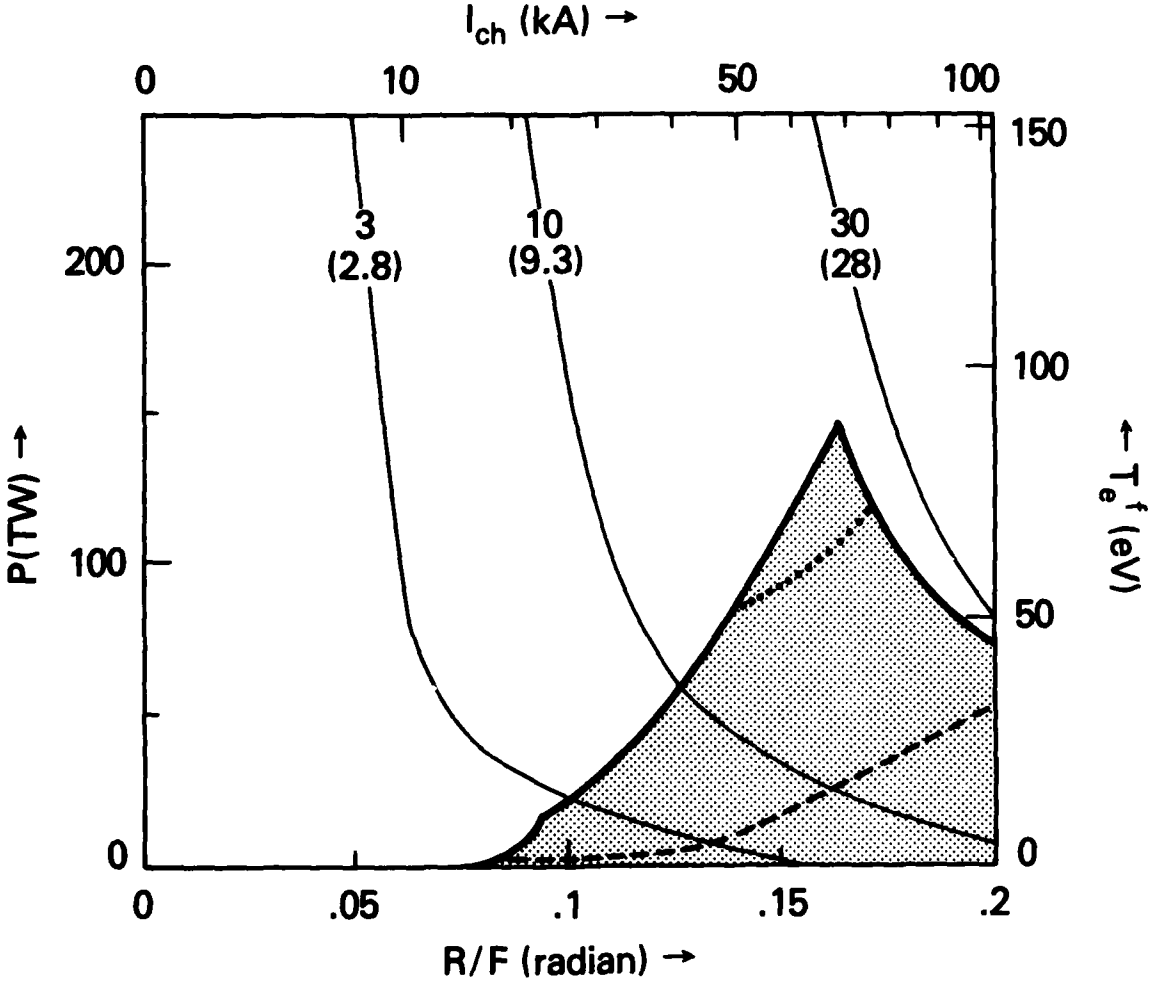

Figure 13 - Operational transport window for a H^{+1} beam with x = 2, r_b = 1.5 cm, E_o = 4 MeV and τ_b = 1×10^{-8} s.

Table I – Variation of the five transport constraints with increasing A_b, x, r_b, E_o, τ_b^{-1} and Z_b. A "+" means the constraint is relaxed, an "0" means there is no change and a "–" means the constraint becomes more severe.

	P_{ES}	θ_{BF}^{-1}	P_{CF}	P_{MHD}	$P_{\delta E}$	Comments
A_b	+	+	+	0	0	source availability and purity limitations
x	+	0	+	+	-	x > 1 is assumed
r_b	+	0	0	+	+	final focusing limitations
E_o	+	-	+	+	+	acceptable range defined by target designs
τ_b^{-1}	+	0	-	+	+	limited to no less than the pellet implosion time
Z_b	-	+	-	0	0	usually fully stripped by foils

6. REFERENCES

1. S. A. Goldstein and R. Lee, Phys. Rev. Lett. 35,1079 (1975).

2. J. W. Poukey, J. R. Freeman, M. J. Clauser, and G. Yonas,. Phys. Rev. Lett. 35,1806 (1975).

3. J. W. Poukey, J. Vac. Sci. Technol. 12, 1214 (1975).

4. A. E. Blaugrund, G. Cooperstein, J. R. Boller and S. A. Goldstein, Bull. Am. Phys. Soc. 20, 1252 (1975).

5. P. A. Miller, C. W. Mendel, D. W. Swain, and S. A. Goldstein, in Proceedings of the International Topical Conference on Electron Beam Research and Technology, Albuquerque, NM (1975), p. 619.

6. G. Cooperstein, S. J. Stephanakis, J. R. Boller, R. Lee, and S. A. Goldstein, in Proceedings of the 1976 IEEE International Conference on Plasma Science, Austin, Texas (IEEE, New York, 1976), p. 126.

7. D. J. Johnson, G. W. Kuswa, A. V. Farnsworth, Jr., J. P. Quintenz, R. J. Leeper, E. J. T. Burns and S. Humphries, Jr., Phys. Rev. Lett. 42, 610 (1979); D. J. Johnson, Bull. Am. Phys. Soc. 24 925 (1979).

8. G. Cooperstein, S. A. Goldstein, D. Mosher, W. F. Oliphant, F. L. Sandel, S. J. Stephanakis and F. C. Young, in Proceedings of the Third International Topical Conference on High Power Electron and Ion Beam Research and Technology, Novosibirsk, USSR (1975).

9. G. Cooperstein, S. A. Goldstein, D. Mosher, R. J. Barker, J. R. Boller, D. G. Colombant, A. Drobot, R. A Meger, W. F. Oliphant, P. F. Ottinger, F. L. Sandel, S. J. Stephanakis and F. C. Young, in Laser Interaction and Related Plasma Phenomena, edited by H. Schwarz, H. Hora, M. Lubin and B. Yaakobi, (Plenum Press, New York, 1980).

10. R. O. Bangerter and D. J. Meeker, in Proceedings of the Second International Topical Conference on High Power Electron and Ion Beam Research and Technology, Ithaca, New York (1977), p. 183; J. H. Nuckolls, in Proceedings of the Topical Meeting on ICF (Opt. Soc. of Am. Wash., DC, 1978) paper TuA5; S. Jorna and N. Metzler, Conference Recond-Abstract of the 1980 IEEE International Conference on Plasma Science, Madison, Wisconsin (IEEE, New York, 1980), p.37.

11. S. A. Goldstein, D. P. Bacon, D. Mosher and G. Cooperstein, in Proceedings of the Second International Topical Conference on High Power Electron and Ion Beam Research and Technology, Ithaca, New York (1977), p. 71; F. L. Sandel, Bull. Am. Phys. Soc. 26, 998 (1981).

12. D. Mosher, G. Cooperstein and S. A. Goldstein, in Proceeding of the Topical Meeting on ICF, San Diego (Opt. Soc. of Am., Wash., DC 1980), p. 104.

13. D. Mosher, Bull. Am. Phys. Soc. 24, 926 (1979).

14. D. Mosher and S. A. Goldstein, Bull. Am. Phys. Soc. 23, 800 (1978).

15. P. F. Ottinger, S. A. Goldstein and D. Mosher, in Conference Record-Abstracts of the 1980 IEEE International Conference on Plasma Science, Madison, Wisconsin (IEEE New York, 1980), p. 95; P. F. Ottinger, D. G. Colombant, S. A. Goldstein, R. A. Meger and D. Mosher, Bull. Am. Phys. Soc. 26, 921 (1981); R. A. Meger, S. A. Goldstein, P. F. Ottinger, D. Mosher, S. J. Stephanakis and F. C. Young, Bull. Am. Phys. Soc. 26, 921 (1981).

16. D. G. Colombant, D. Mosher and S. A. Goldstein, Phys. Rev. Lett. 45, 1253 (1980); D. G. Colombant and S. A. Goldstein, NRL Memorandum Report 4640 (1981).

17. P. F. Ottinger, D. Mosher and S. A. Goldstein, Phys. Fluids 23, 909 (1980).

18. D. Mosher, D. G. Colombant and S. A. Goldstein, Comments Plasma Physics 6, 101 (1981).

19. P. F. Ottinger, D. Mosher and S. A. Goldstein, Phys. Fluids 22, 332 (1979).

20. P. F. Ottinger, D. Mosher and S. A. Goldstein, Phys. Fluids 24, 164 (1981).

21. P. F. Ottinger, in Conference Record-Abstracts of the 1980 IEEE International Conference on Plasma Science, Madison, Wisconsin (IEEE, New York, 1980), p. 57.

22. P. F. Ottinger, S. A. Goldstein and D. Mosher, NRL Memorandum Report 4548 (1981).

23. P. F. Ottinger, S. A. Goldstein and D. Mosher, NRL Memorandum Report 4180 (1980).